Pharmaco-fUS: Quantification of pharmacologically-induced dynamic changes in brain perfusion and connectivity by functional ultrasound imaging in awake mice

Claire Rabut, Jérémy Ferrier, Adrien Bertolo, Bruno Osmanski, Xavier Mousset, Sophie Pezet, Thomas Deffieux, Zsolt Lenkei, Mickaël Tanter

NeuroImage 222 (2020) 117231

Contents lists available at ScienceDirect

NeuroImage

journal homepage: www.elsevier.com/locate/neuroimage

Pharmaco-fUS: Quantification of pharmacologically-induced dynamic changes in brain perfusion and connectivity by functional ultrasound imaging in awake mice

Claire Rabut[a], Jérémy Ferrier[b], Adrien Bertolo[c], Bruno Osmanski[c], Xavier Mousset[a], Sophie Pezet[a], Thomas Deffieux[a], Zsolt Lenkei[b,#], Mickaël Tanter[a,#,*]

[a] Physics for Medicine Paris, Inserm, ESPCI Paris, CNRS, PSL Research University - Paris, France
[b] Institute of Psychiatry and Neurosciences of Paris, University of Paris, INSERM U1266, 102 rue de la Santé, 75014 Paris, France
[c] Iconeus, 6 Rue Calvin, 75005 Paris, France

ARTICLE INFO

Keywords:
Functional ultrasound imaging
Awake imaging
Functional biomarker
Support Vector Machine classifier
Drug effects monitoring

ABSTRACT

There is a critical need for reliable quantitative biomarkers to assess functional brain alterations in mouse models of neuropsychiatric diseases, but current imaging methods measuring drug effects through the neurovascular coupling, face issues including poor sensitivity, drug-induced changes in global brain perfusion and the effects of anesthesia.

Here we demonstrate the proof-of-concept of a minimally-invasive fUS imaging approach to detect the acute cholinergic modulatory effects of Scopolamine (ScoP) on functional brain connectivity in awake and behaving mice, through the intact skull. A machine-learning algorithm constructed an ad-hoc pharmacological score from the ScoP-induced changes in connectivity patterns of five mice. The discrimination model shows important ScoP-induced increase of the hippocampo-cortical connectivity. The pharmacological score led to robust discrimination of ScoP treatment from baseline in an independent dataset and showed, in another independent group, dose-dependent specific effects of central cholinergic modulation of functional connectivity, independent from global brain perfusion changes. In conclusion, we introduce pharmaco-fUS as a simple, robust, specific and sensitive modality to monitor drug effects on perfusion and functional connectivity in the awake mouse brain.

1. Introduction

Development of new drugs for brain disorders is challenged both by the lack of precise understanding of drug effects on brain function and by the paucity of validated preclinical models. Functional MRI (fMRI), by providing direct readout of brain activation and connectivity patterns through the neurovascular coupling, has been proposed as an interesting tool both in pre-clinical and clinical drug development (Carmichael et al., 2018; Nathan et al., 2014; Wandschneider and Koepp, 2016) a technique referred to as 'pharmacological MRI' or 'pharmaco-fMRI' (phMRI). However, pre-clinical use of phMRI is strongly limited by the requirement for immobilization or anesthesia and by low sensitivity, especially in mice, a major pre-clinical rodent model. In addition, the current gold standard method of phMRI, BOLD (blood oxygenation-level dependent) imaging cannot measure another important confounding factor - changes in global brain perfusion. Nuclear imaging techniques such as PET offer the sensitivity required to monitor drug distribution, pharmacokinetics and pharmacodynamics. PET is also a largely used tool in central nervous system drug discovery and development (Halldin et al., 2001; Piel et al., 2014), partly due to a growing list of neuroreceptor-specific PET tracers and the growing availability of small-animal PET cameras (Cherry, 2001). A significant number of small-molecule receptor ligands have been labelled with 11C and 18F, and some of these ligands readily cross the blood–brain barrier and bind to their intended targets. This labelling does not affect the chemical properties of the studied compound, allowing the monitoring of the drug biodistribution. It is extremely sensitive (up to picomoles concentration) but relies on limited spatial and temporal resolutions.

Based on ultrasensitive Doppler imaging, functional ultrasound (fUS) imaging provides an emerging method for imaging brain activation by directly measuring cerebral blood volume (CBV) changes induced by neurovascular coupling (Macé et al., 2011). It allows the study of dynamic brain activation patterns with a large field of view and has been used successfully in animal models, from awake rats

* Corresponding author.
E-mail address: mickael.tanter@espci.fr (M. Tanter).
Co-senior authors.

https://doi.org/10.1016/j.neuroimage.2020.117231
Received 24 May 2020; Received in revised form 24 July 2020; Accepted 31 July 2020
Available online 12 August 2020

(Sieu et al., 2015) to behaving primates (Dizeux et al., 2019). fUS imaging also enables to measure functional connectivity in rodents (Osmanski et al., 2014). While we have recently demonstrated fUS imaging of functional brain activation in freely moving awake mice (Tiran et al., 2017), currently we do not know whether fUS would be useful for robust, specific and quantitative (i.e. dose-dependent) imaging of pharmacologically-induced changes in brain activation and connectivity in the awake mouse brain, which allows to avoid anesthesia-induced bias.

In this proof-of-concept study of Pharmacological functional Ultrasound (Pharmaco-fUS), we aimed to reveal time- and dose-dependent functional connectivity modulations in awake mice, after the administration of scopolamine, a widely used psychoactive compound that modifies cholinergic neurotransmission (Deutsch, 1971), which is thought to be involved in the physiopathology of Alzheimer's disease. After the establishment of a novel awake-fUS imaging setup, we have focused on the development and validation of a machine-learning approach, which, by using the rich data content provided by fUS connectivity imaging, would enable to obtain a reliable 'fingerprint' of scopolamine-induced changes in brain connectivity. This 'scopolamine fingerprint' could be used to better understand neuronal mechanisms of cholinergic modulation and, by comparing it to control, to develop and validate novel pharmacological compounds of therapeutic value.

2. Materials and methods

2.1. Animals

Mice were housed four per cage in a controlled environment and were provided with food and water ad libitum. To minimize stress during the experimental procedure, mice were given a 7-day acclimation period after their arrival. All animals received human care in compliance with the European Communities Council Directive of 2010. This study was approved by the local committee for animal care (Comité d'ethique en matière d'expérimentation animale N°59) under Agreement #19847-201711172358582v4. Experiments were carried out in C57Bl/6 male mice (Janvier Labs), 7-week-old at the beginning of the experiment's procedure (starting with the implantation of metal frame on the skull). All efforts were made to minimize animal suffering.

2.2. Implantation of metal frame

Eight to ten days before the fUS imaging acquisition session on awake freely moving mice, a flat metal frame was fixed on the mouse skull to enable the magnetic fixation of the ultrasonic probe (Fig. 1a-c), following the same procedure than previously described (Tiran et al., 2017). For the surgical implantation of the metal frame, mice were anesthetized using a mixture of ketamine (100 mg/kg, intraperitoneal (ip)) and medetomidine (1 mg/kg, ip) and placed on a stereotaxic frame. After verifying the loss of pedal withdrawal reflex, the skin and periosteum were removed to expose the skull. The metal frame, aimed to stabilize a miniaturized ultrasonic probe in a magnetized probe holder (Fig. 1a.b) during the acquisition sessions, was fixed on the skull with two surgical anchoring screws (Fig. 1c). The stability of the metal frame was further ensured using dental cement (Dental Adhesive Resin Cement - Super bond C&B). The frame window (ranging roughly from the skull landmarks Bregma to Lambda) was covered with Silicon Elastomer Kwik Cast® (World Precision Instruments) to ensure protection and maintain integrity of the bone. Anesthesia was then reversed with a subcutaneous injection of atipamezole (1 mg/kg, Antisedan). All mice received a prophylactic administration of antibiotics (Borgal 24%, 0.6 ml/kg/day, subcutaneous (s.c.)) and meloxicam (Metacam 5 mg/kg/day, s.c.) to prevent post-operative pain. The mice were left for two days to recover from this procedure. Mice carry chronically only the metal frame and two screws, corresponding to a total weight of 1.4 g. The normal activity of the mice was not notably disturbed.

2.3. Functional ultrasound imaging

Imaging procedure, acquisitions were performed using a 15 MHz ultrasonic ultralight probe prototype (15 MHz, 64 elements, 0.110 mm pitch, Vermon, Tours, France) (Fig. 1a) connected to a prototype ultrafast research ultrasound scanner with real-time neuro-imaging software (Neuroscan, Iconeus, Paris, France). The prototype implemented real-time transcranial functional ultrasound (Mace et al., 2013). Each image was obtained from 200 compounded frames acquired at 500 Hz frame rate, using 11 tilted plane waves separated by° 2 (-10°,-8°,-6°,-4°,-2°, 0°, 2°, 4°, 6°, 8°,10°) acquired at a 5500 Hz pulse repetition frequency (PRF). Imaging sessions could last as long as needed (typically one hour and half) and were performed by real-time continuous acquisitions of successive blocks of 400 ms of compounded plane wave imaging. Each block was processed using a SVD clutter filter (Demené et al., 2015) to separate tissue signal from blood signal to obtain a power Doppler image.

2.4. Imaging procedures on awake mice

Main preclinical imaging modalities require the immobility of the subject which necessitates the restraining or the sedation of animals. Both anesthesia and constriction-induced stress inevitably affect cerebral activity and putatively interfere with data interpretation. To enable transcranial whole-depth brain imaging in awake behaving mice, we used a miniaturized prototype ultrasonic probe (Fig. 1a), placed in an adjustable magnetic probe holder (Fig. 1b), which, after being clipped on a metal frame chronically fixed on the intact mouse skull by minimally invasive surgery (Fig. 1c), allows the choice of the transcranial imaging plane for each imaging session. Therefore fUS allows to study behaving animals, however further steps of data and signal filtering are necessary to remove motion artefacts recorded in the awake mouse (see Section 2.6.1. *Frames removal, filtering and motion regression*).

Mice were placed in a home-made box freely rolling around on beads, which prevented excessive twisting of the transducer cable by allowing the cage to freely rotate and allowed relatively free motion of the animals during fUS imaging sessions (Fig. 1d). This hybrid configuration between freely-moving and head-fixed setups gave the best compromise in terms of motion and head restraints. After a resting period and a couple of training sessions (**Supplementary Fig.1a**), mice were habituated to remain up to 3h in the setup, with the probe fixed on their head.

In order to select the adequate imaging plane, each mouse was first rapidly anesthetized with isoflurane (1.5%). The Kwik-Cast® layer protecting the skull was removed and the skull was cleaned with saline. After magnetically clipping the probe-holder, its position was manually adjusted with small screws using the real-time image of the transcranial Doppler images. For all this study, we acquired images at the coronal plane at Bregma -2.3 mm. The choice of this coronal plane was motivated by the results from previous studies based on histology analysis (J-C. Lee et al., 2018; J-S Lee et al., 2016; Park et al., 2016) or fMRI (Sperling et al., 2002; Wink et al., 2006) showing that scopolamine induced-effects and recovery-effects in mice were significantly noticeable in hippocampus, notably because of the memory impairment caused by scopolamine. When required, and before starting acquisition, the mouse was left to recover from the isoflurane for at least 30 min inside the mobile-box with the probe attached. Acquisitions were started after this initial recovery period, as soon as the mouse was quiet and behaved normally.

In order to study the functional connectivity at genuine resting-state periods, we analyzed time periods where the mice were not actively moving (see Section *2.6.2 Extracting quiet time periods*).

2.5. Pharmacological studies

Longitudinal study: We first investigated the pharmacodynamics of functional connectivity changes induced by 3 mg/kg scopolamine in a

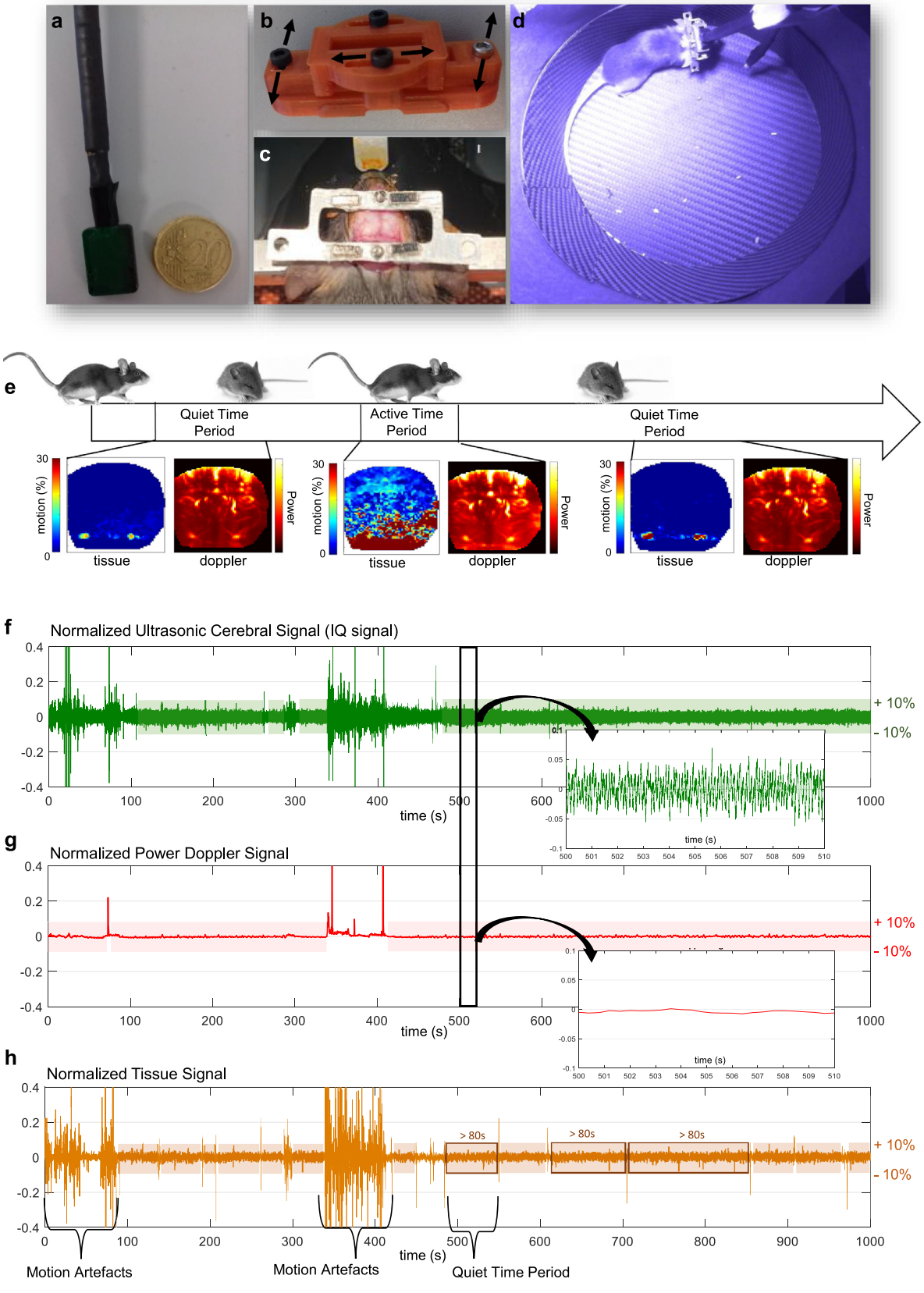

Fig. 1. Awake fUS imaging setup and the method for the limitation of motion artifacts. a) Miniaturized ultrasonic probe b) Adjustable magnetic probe holder. c) Metal frame chronically fixed on the mouse's skull. Screws were positioned in front of the Bregma and behind the Lambda points. The field of view is approximately 5mm wide. d) Image of a mouse freely moving in the rolling-box. (e-h): Example of a selection of a quiet time period e) Three representative periods of the mouse activity during recording. We can separate the tissue motion from the Doppler signal. The tissue motion admits high values all over the brain during the mouse active time whereas this motion is hardly detectable in the Doppler signal. f) Normalized Ultrasonic Cerebral Signal (also called 'IQ signal'), without filtering, representing all the backscattered echoes received from the brain. g) Normalized pPower Doppler signal (after SVD filtering to remove the first modes of energy in a new spatio-temporal orthogonal base (Demené et al., 2015), showing the temporal course of the CBV signal. The black rectangle focuses on a 10 s period where the standard deviation of both normalized signals doesn't exceed 10%, defining it as a quiet temporal period. h) Confirmation of the time period selection by analysis of the tissue signal: when normalized, the time course of the tissue signal during the selected time period should also admit a standard deviation under 10%. The time slots that formed a successive uninterrupted period of 80 seconds (to avoid fragmented or small individual periods) were used for the functional connectivity analysis.

group of 5 mice. For this study, we first performed a 30 min continuous baseline acquisition of the cerebral perfusion of awake mice. We then injected subcutaneously 300 μL of scopolamine (3 mg/kg) to the awake mouse and acquired hemodynamic activity during one h, starting 15 min after scopolamine injection (**Supplementary Fig.1b**).

Dose-response Study: We next investigated the dose-dependence, as well as the effects of post-scopolamine treatment with the muscarinic acetylcholine receptor agonist milameline and the effects of a peripherically-restricted scopolamine derivative: methyl-scopolamine (Andrews et al., 1994). This study was performed on six different groups of mice. Four doses of scopolamine were tested (0.1 mg/kg; 0.2 mg/kg; 0.5 mg/kg: 3 mg/kg; *n*=5 per group). One group received an injection of 300 μL of saline (group 0) and a last group (group 5) received a dose of methyl-scopolamine (1 mg/kg, *n*=4 mice per group). All those groups of mice were subjected to the following protocol (**Supplementary Fig.1.c**): a first 30 min baseline pharmacological set of fUS images were acquired, after which saline, scopolamine (0.1 mg/kg; 0.2 mg/kg; 0.5 mg/kg; 3 mg/kg) or methyl-scopolamine (3 mg/kg) (all injected volumes: 0.3 ml) was subcutaneously (s.c.) administered. After 15 min another 30 min of fUS images was acquired. Then, the mice were injected with milameline (1 mg/kg, s.c.) except for group 0, and a last 30min fUS-acquisition was performed 15 min after the milameline injection (all injected volumes 0.2 ml).

Methyl-scopolamine is a methylated derivative of scopolamine. It presents the same receptor binding characteristics as scopolamine but does not cross the blood–brain–barrier. Methyl-scopolamine can be used as a control drug at the same dose than scopolamine, for behavioral studies using scopolamine (Shah et al., 2015).

2.6.1. Frames removal, filtering and motion regression

While using head-fixed probes fUS imaging is much less sensitive to motion artifacts than fMRI and although the use of the rolling box further smoothens the effect of sudden movements, motion artifacts may still remain in the Doppler signal. As they appear in several brain structures at the same time, those artifacts can lead to artificially high correlations between structures which are not due to neural signals but to motion. To mitigate those effects in our results, several steps were necessary. First, we used an advanced clutter filter based on singular value decomposition to separate blood motion from tissue motion using spatio-temporal coherence (Fig. 1e). Previously, this filter was shown to be a robust tool to reduce movement artifacts in several scenarios (Demené et al., 2015). Secondly, we identified frames to be removed from each acquisition by using a combination of thresholds - a first threshold on Doppler signals chosen at +/-10% of the median value (Fig. 1g) and a second threshold using a tissue velocity estimator based on beamformed IQ data (Kasai et al., n.d.) and chosen at +10% above the baseline (Fig. 1.h). Thirdly, of all remaining frames we only kept frames that formed a successive uninterrupted period of 80 s, to avoid fragmented or small individual periods.

We then applied a low-pass filter at 0.2 Hz to remove high frequency signals while preserving the resting-state frequency band. The signal was then detrended with a polynomial fit of order 4 to remove low frequency fluctuations. Finally, singular value decomposition of the data was performed. Since the first spatial eigenvector is coupled to the whole brain tissue, it was systematically removed. Although this form of global signal regression can lead to anti-correlation values between structures that may be difficult to interpret, it was preferred to avoid any remaining global motion signal that can affect the whole brain tissue and induce artificially strong correlations.

2.6.2. Extracting quiet time periods

Longitudinal study: for each of the 5 mice, we were able to extract from their longitudinal acquisitions seven different blocks of useful signal lasting from 80 to 120 s (as defined in the previous paragraph *Frames removal, filtering and motion regression*) and corresponding to seven distinct periods of the acquisition: two periods prior scopolamine injection T1 and T2, and four successive periods post scopolamine injection from T3 to T7. The time ranges of those periods are detailed in Table 1 and presented in Fig. 2.

Period	Acquisition	Range
T1	Baseline	T= 2min -> 6min
T2	Baseline	T= 22min -> 26min
T3	After Scopolamine	T= 1min -> 5min
T4	After Scopolamine	T= 13min -> 17min
T5	After Scopolamine	T= 28min -> 31min
T6	After Scopolamine	T= 44min -> 47min
T7	After Scopolamine	T= 55min -> 60min

Dose-response study: for each group, we extracted from their longitudinal acquisitions one block of a time period ranging from 80s to 200s in each pharmacological state (i.e. baseline state, after scopolamine injection, after milameline injection, …).

2.6.3. Seed-based analysis

Seed-based maps were also calculated estimated from the correlation over time of the time course of the CBV signal extracted from a small selected ROI (the seed region as defined by the operator), with signals from all the other pixels of the brain. Two different seeds were chosen: the left hippocampus (seed S_h) and the left frontal cortex (seed S_c) both at the level of Bregma -2.3mm.

2.6.4. Functional connectivity matrices

In order to build functional connectivity matrices [M], we used the time course of the CBV signal extracted from 10 different ROIs defined from the Paxinos Atlas (Ketih Franlkin, 2011) (See Fig. 2c for ROIs location). We then determined the Pearson correlation between each filtered ROIs' signal and report the correlation coefficients on a 10×10 matrix. At the intersection of the i^{th} line and j^{th} column, the value of the cell $M_{i,j}$ of the matrix **M** is the correlation coefficient between the region $n^{\circ}i$ and the region $n^{\circ}j$.

2.6.5. Hippocampo-cortical correlation score

The hippocampo-cortical correlation score evaluates the correlation between the regions of interest (ROIs) located in the cortex (regions 1 to 6) and the regions of the hippocampus (regions 7 and 8). It corresponds to the mean value of the cells from the connectivity matrices expressing the hippocampo-cortical correlation, i.e. cells of coordinates: (7,1); (7,2); (7,3); (7,4); (7,5), (7,6); (8,1); (8,2); (8,3); (8,4); (8,5); (8,6)

2.6.6. Pharmacological fUS statistics

Paired T-tests were used to compare baseline, post-scopolamine and post-milameline injection scores for the different studied groups (Fig. 3.d & Fig. 5.b). Similarly, paired T-tests were used to compare the baseline, scopolamine and milameline hippocampo-cortical scores for the different studied groups (**Supplementary Fig.3**). For the statistical threshold significance for p values, we apply the following convention (followed by the APA (American Psychological Association) and the NEJM (New England Journal of Medicine)):

$p > 0.05$: non-significant (ns)
$p < 0.05$: significant (*)
$p < 0.01$: very significant (**)
$p < 0.001$: extremely significant (***)

Significance values however, were not corrected for multiple-comparisons.

2.6.7. Statistical analysis using a Support Vector Machine model

We trained a linear regression model (Support Vector Machine (SVM) type) to recognize in an unbiased way the connectivity changes due to scopolamine injection in a first dataset. The goal of an SVM classifier is to learn how to determine a border between two training categories. In an N-dimensional space, two sets of (training) points of N

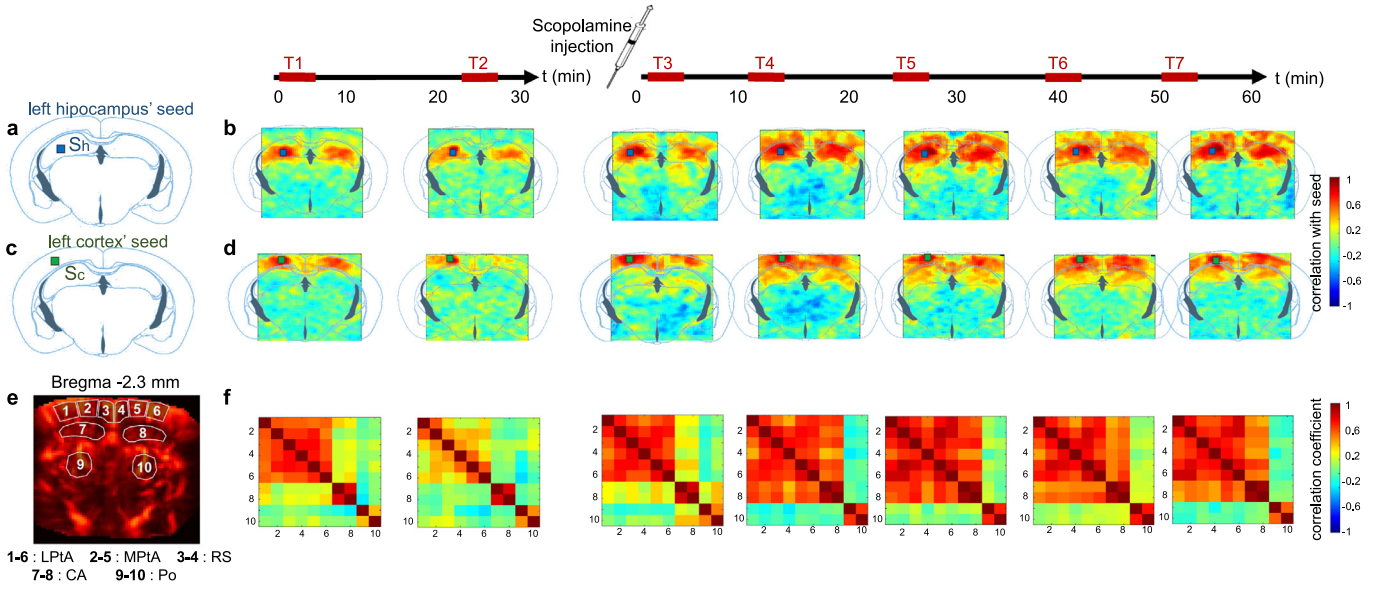

Fig. 2. Longitudinal effects of a single-dose scopolamine injection on cerebral connectivity. After a baseline imaging acquisition at the Bregma -2.3mm coronal plane during 30min, 300µl of scopolamine was subcutaneously injected at a 3 mg/kg dose, followed by continuous imaging acquisition of one hour. Seven motion-free time periods (two baseline T1-T2, and 5 post-scopolamine T3-T7) were selected to analyze the dynamic evolution of connectivity. a-b) Longitudinal analysis of connectivity of the hippocampal seed (Sh) positioned in (a) the left hippocampus and of the cortical seed (Sc) positioned in (b) the left cortex. c-d) Mean seed-based analysis correlation maps (averaged over 5 mice): longitudinal analysis of connectivity of the cortical seed (Sc) positioned in the left placed in the left lateral parietal associatif (L-PtA) cortex. e) 10 regions of interest (ROIs) are selected to represent the connectivity patterns using connectivity matrices: 1-6: lateral parietal association cortex (LPtA); 2-5: medial parietal association cortex (MPtA); 3-4: retrosplenial granular and dysgranular cortex (RS); 7-8: hippocampus (CA); 9-10: posterior thalamic nuclear group (Po). f) Mean connectivity matrices at each time period showing pair-wise temporal correlations between the signal of the 10 selected ROIS.

coordinates belonging to two different categories will be separated by linear regression by an "optimal" hyper-line. This line (of N dimensions) corresponds to the border farthest from all the points: it is said to have the "best generalization capacity".

We trained our model with the correlation matrices of size 10 × 10 of the five mice used during the pharmacodynamic study to find this optimal border between the two pharmacological states. In total 10 matrices: five matrices at baseline state and five matrices for scopolamine-treatment were used. We assigned a score = 0 to the baseline matrices and a score = 1 to the matrices of animals treated with scopolamine (Fig. 3a).

Knowing the **score** (**0** or **1**) of each connectivity matrix **C** of the training groups (baseline matrices or scopolamine matrices), the SVM algorithm calculated the optimal hyper-line **A** of the equation **score**=f(**C**) (Fig. 3b).

The resulting hyper-line is a 10 × 10 matrix **A** so that:

$$\mathbf{score} = \mathbf{C}.\mathbf{A} + \mathbf{b}$$

(where b is the y-intercept of the hyper-line C and b=0.1575)

Each cell $A_{i,j}$ of **A** represents the optimal point maximizing the distance between the cells $B_{i,j}$ from the matrices of the baseline group and the cells $S_{i,j}$ from the matrices of the scopolamine group.

Then, to validate the score of the second cohort of mice (which is independent of the training cohort), we considered the inverse problem and calculated for each connectivity matrix **C'** to evaluate the estimated score according to the SVM model (Fig. 3.c.d).

2.6.8. Cross-validation

To evaluate the stability of the presented results, we subjected our SVM-model to cross-validation. To do so, we randomly picked 100 combinations of 5 training matrices and 8 validation matrices among the 13 correlation matrices (5 from the mice of the training cohort, 8 from the mice of the validation cohort) used for to establish and validate the SVM model at first (Fig. 4.a). The same linear regression model was used to calculate 100 hyper-lines **C** optimizing the border between the baseline states and scopolamine states of the 5 randomly picked training matrices. The mean SVM-coefficient matrix is represented in Fig. 4b.

The performance of the cross-validation model is represented with the mean Receiver Operating Characteristic (ROC) curve of Fig. 4c. The ROC curves of each random sampling represent the diagnostic ability of our classifier to discriminate the baseline states from the pathological states. We create here the mean ROC curve by calculating for each sampling (and then averaging by the number of sampling) the true positive rate function of the false positive rate at various threshold settings. Four indices for each sampling evaluate the adequacy of the model:

Area Under Curve (AUC): area under the ROC curve, linearly correlated to the performance of the model.
Accuracy: (number of correctly estimated scopolamine matrices and correctly estimated baseline matrices)/(total number of matrices)
Sensitivity: (number of correctly estimated scopolamine matrices) / (total number of scopolamine matrices).
Specificity: (number of correctly estimated baseline matrices) / (total number of baseline matrices)

The mean AUC, Accuracy, Sensitivity and Specificity averaged over the 100 trials are displayed in Fig. 4c.

2.7. Code accessibility and data availability

The data that support the findings of this study, including preprocessing and analysis scripts, are available in an open repository: https://sandbox.zenodo.org/record/558582.

3. Results

3.1. Longitudinal effects of a single-dose scopolamine injection on cerebral connectivity

Using the awake fUS imaging setup described in 2.4, we first investigated the pharmacodynamics of functional connectivity changes induced by 3 mg/kg scopolamine in a group of 5 mice. The scopolamine

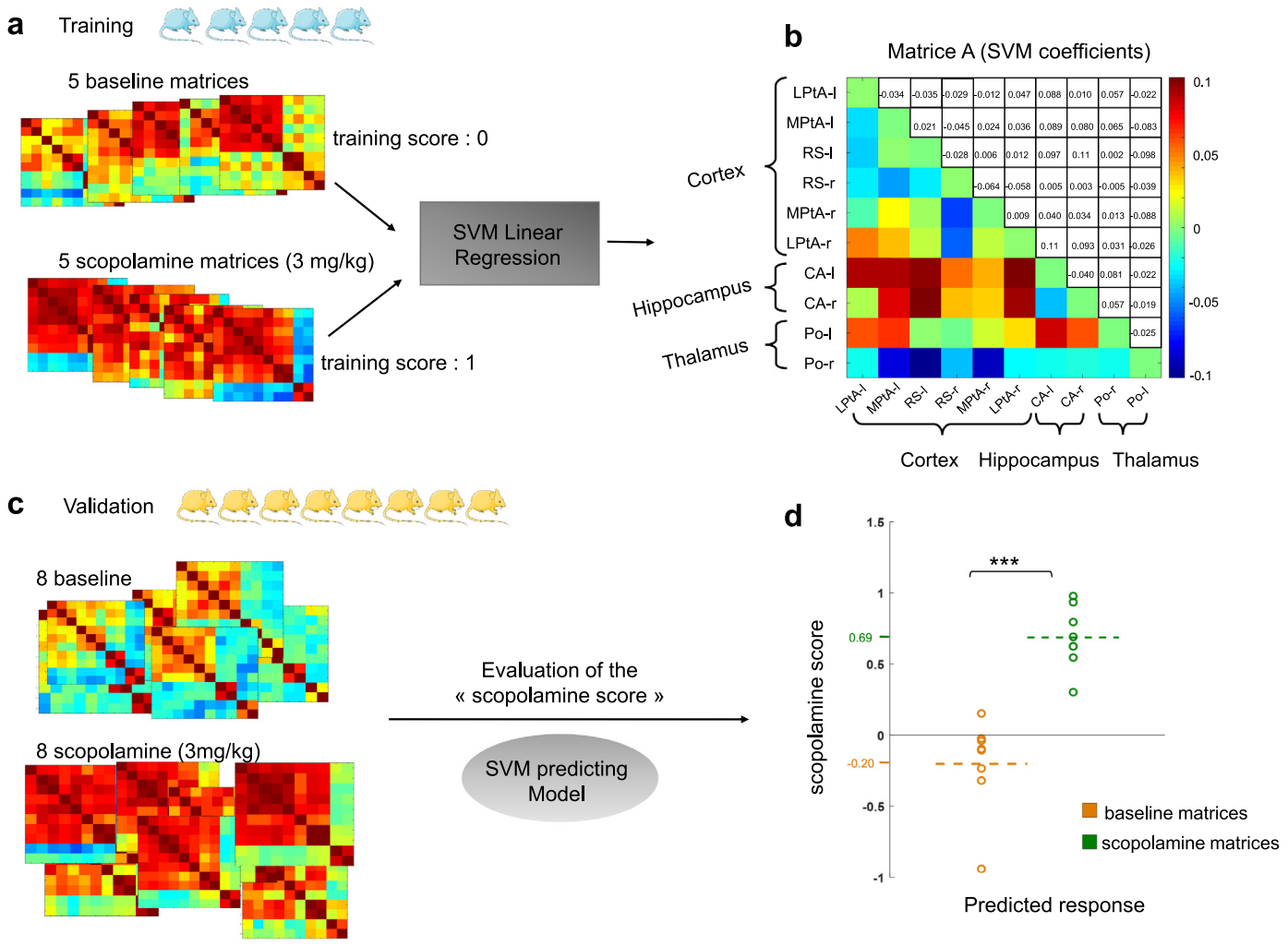

Fig. 3. Automatic detection of pharmacologically-induced connectivity changes a) We trained the SVM linear model with 10 sets of data: 5 baseline connectivity matrices assigned with a score 0 ("baseline state") and 5 scopolamine matrices assigned with a score of 1 ("pathological state") b) SVM-coefficient matrix associated to the trained model: values of individual cells indicate their importance in the discrimination of the two training groups. Notably, most cells of the hippocampo-cortical correlation display high values. ROIs: 1-6: lateral parietal association cortex (LPtA); 2-5: medial parietal association cortex (MPtA); 3-4: retrosplenial granular and dysgranular cortex (RS); 7-8: hippocampus (CA); 9-10: posterior thalamic nuclear group (Po)(l=left; r=right) c) Validation of the predicted model on a second independent cohort of mice which have undergone the same experimental protocol. d) Prediction of the "scopolamine score" of the 16 validation matrices, by using the trained model. At baseline state: $\mathbf{score_{SVM}} = -0.20$. After scopolamine injection: $\mathbf{score_{SVM}} = 0.69$ ($\mathbf{p} = 0.0004$). Graph: mean ± single score.

dose used for this experiment is in the typical range for rodent models (Deng et al., 2019; Guo et al., 2016; Haider et al., 2016; Lin et al., 2016; Muhammad et al., 2019; Shah et al., 2015; Xu et al., 2016). At baseline state, we selected two motion-free periods, the first from the 0-10 minutes period (labeled T1 on Fig. 2) and the second from the 20-30 minutes period (T2). After subcutaneous scopolamine injection, we selected motion-free analysis periods from every 10 minutes ranges of acquisition (T3-T7, **Supplementary.Fig.1**).

In order to compare fUS imaging with conventional pharmacological studies based on the variation of baseline CBV or BOLD signal, we first studied the global cerebral flow baseline variations after scopolamine injection in two control groups of N=5 mice. Although we recognize the low sampling size of these two groups, we did not measure significant change of global CBV baseline after scopolamine injection (**Supplementary Fig.2a**).

We used seed-based analysis to evaluate the correlation of the CBV signal between all pixels of the imaging plane and two seed regions: a hippocampal seed (*Sh*), placed in the left dorsal hippocampus and a cortical seed (*Sc*), placed in the left lateral parietal association (LPtA) cortex (Fig. 2a,c). Before the scopolamine injection (time-points T1 and T2), the two hippocampi were the only regions correlating with *Sh* (Fig. 2a-b), and the cortical regions were only strongly correlating with *Sc* (Fig. 2c-d), illustrating the powerful interhemispheric connections between these structures. Right after the scopolamine injection (time T3, corresponding to the 0-10 minutes post-injection period), the seed-based maps did not show notable difference as compared to baseline (T1 and T2). However, increase both in interhemispheric and hippocampo-cortical correlations can be observed from T4: the cortical regions emerge among the regions strongly correlating with *Sh*. Similarly, *Sc* and both hippocampi presented elevated correlation. At time T5, T6 and T7, this hippocampo-cortical correlation is maintained, suggesting a loss of the intra-regional distinctiveness of the connections (cortico-cortical connections and hippocampo-hippocampal connections).

Next, we extended the analysis of scopolamine-induced changes in functional connectivity to multiple regions of interest (ROIs) at the investigated coronal plane by using correlation matrices (Fig. 2e-f). At baseline time-points (T1-T2), the cortical regions (regions 1 to 6), the hippocampal regions (regions 7 and 8) and the thalamic regions (regions 9 and 10) show high intra-regional correlations, and weak inter-regional

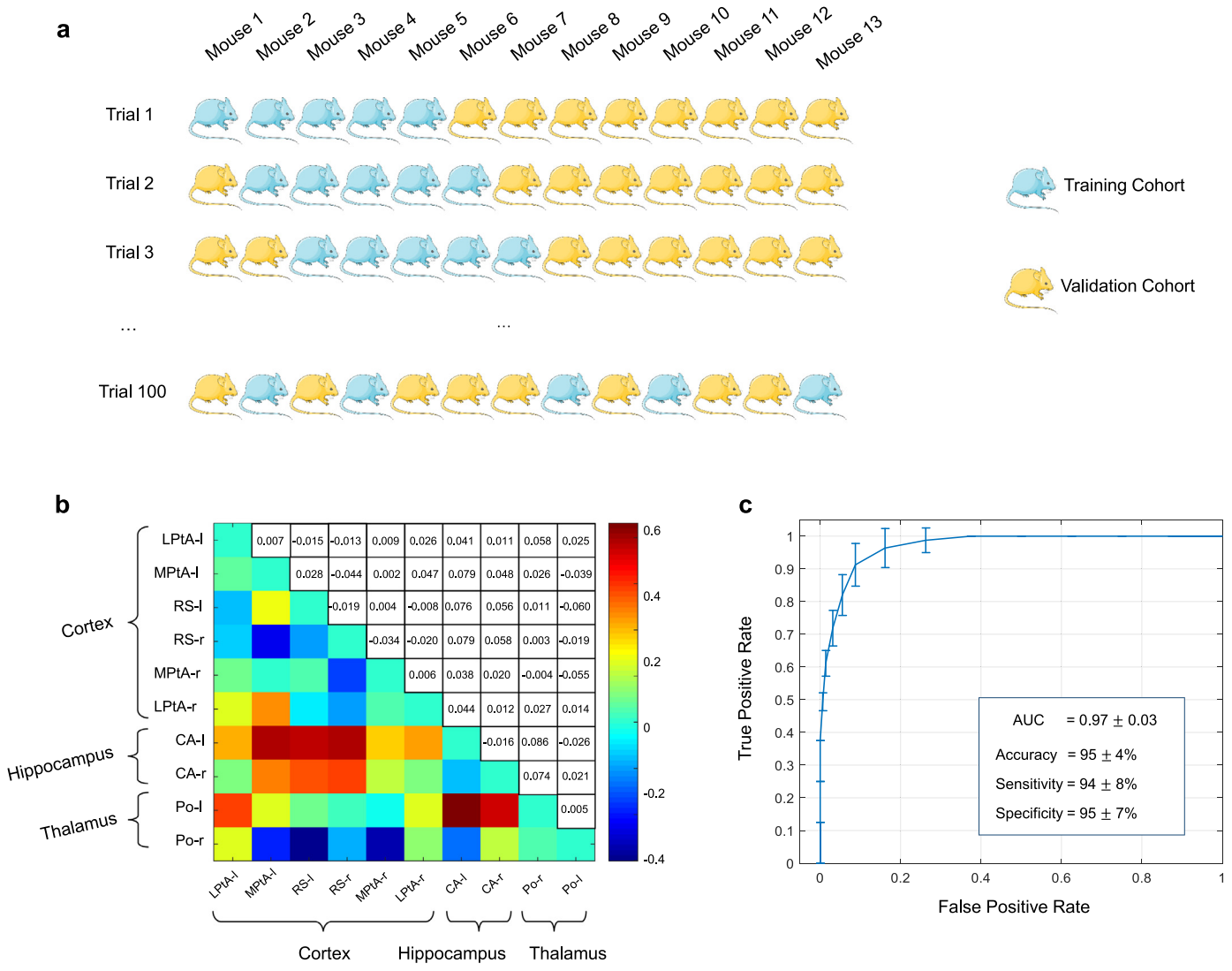

Fig. 4. Cross-validation of the SVM classification model a) Illustrative design of the cross-validation model using 100 iterations. At each trial, a different combination of 5 training mice / 8 validation mice is randomly evaluated. b) Cross validation coefficient matrix average over the 100 trials. c) Cross-validation mean ROC curve. The error bar represents the standard deviation over the 100 trials. d) Circular Graph to illustrate the connectivity connections in a network.

correlations. Starting from T4, similarly to the seed-based analysis, we observed a substantial increase of the correlation coefficients between the ROI's 1 to 6 (cortical regions) and the ROI's: 7 and 8 (hippocampal regions), indicating elevated inter-regional connectivity.

These observations suggest that scopolamine induces an increase of the hippocampo-cortical functional connectivity in mice. While showing clear tendencies, which reached significant levels in several ROI combinations (data not shown), the relatively low number of animals (n=5) in these pilot groups did not provide sufficient statistical power to compensate for the false-positive-result inducing effect of multiple comparisons. The traditional response to this classical problem of under-sampling is to elevate the number of experimental animals, which, by raising ethical, financial and logistic challenges, ultimately hinders the advance of pre-clinical research. We hypothesized that the rich data content of fUS-detected connectivity changes induced by scopolamine at a single coronal section may allow to construct a unique 'score', that could reliably classify animals into control (baseline) and treated groups. Such a score would be useful for pharmaceutical research, through testing of drug candidates by comparing their capacity to rescue pharmacologically-induced pathological connectivity patterns, such as scopolamine-induced hippocampal dysconnectivity, in a reduced number of experimental animals. Indeed, a recent clinical study using machine-learning improved analysis of EEG biomarker data in humans has shown high performance to classify scopolamine-treated vs. non-treated individuals (Simpraga et al., 2017). To confirm this hypothesis, we implemented and then pharmacologically tested a support vector machine (SVM) based automatic classifier algorithm to construct an ad-hoc "scopolamine score". Importantly, the matrix score would indicate and quantify, in a completely unbiased way, the connectivity changes induced by pharmacological compounds that modify brain function.

3.2. Automatic detection of pharmacologically-induced connectivity changes

In order to construct a classifier which would allow the discrimination of scopolamine-induced connectivity patterns from the baseline in awake mice, we trained a support vector machine (SVM) linear regression model algorithm, which aims to maximize the geometric margin between the function and the data. We used the above presented connectivity matrices from time point T1 for baseline (assigned score 0) and time T5 for scopolamine-treatment (score 1) as predictor data (in total 10 matrices, n=5) (Fig. 3.a). After training of the model, we obtained

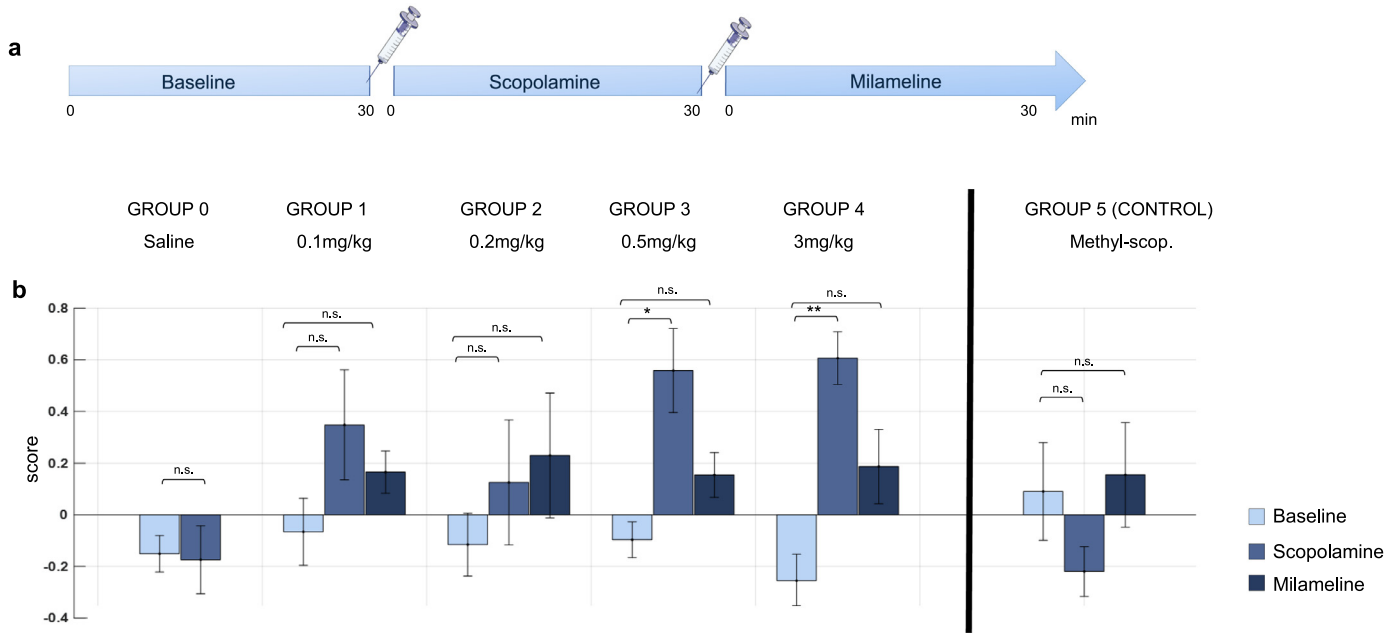

Fig. 5. Pharmacological validation for the automatic detection of scopolamine-induced connectivity changes. a) Schema of the treatment protocol. b) Pharmacological scores obtained in the 5 treatment groups. Groups either received saline (group 0) or increasing doses of scopolamine (groups 1-4) or a single dose of the peripherally-restricted methyl-scopolamine (group 5), followed by a single dose of the antagonist milameline. Paired T-tests were used to compare baseline, post-scopolamine and post-milameline injection scores for the different studied groups (* $p < 0.05$; ** $p < 0.01$). Bar graph: mean ± SEM.

the best values maximizing distances of the intercept b and of the slope **A** in the linear regression calculated upon the equation:

$$\text{score} = \mathbf{C}.\mathbf{A} + b$$

where:

- **C** is a connectivity matrix (variable)
- **A** is a matrix (same size as **C**) which cell's values (noted $A_{i,j}$ for the value of the cell of coordinate (i,j) in the matrix) represent the SVM-coefficients of each cell in the discrimination of the groups. A is bounded between -0.098 and 0.11
- b = 0.1575

Notably, the highest values of **A** were provided by the cells of cortico-hippocampal correlation, in particular: $A_{1,7} = 0.088$, $A_{2,7} = 0.089$, $A_{3,7} = 0.097$, $A_{6,7} = 0.11$, $A_{2,8} = 0.080$, $A_{3,8} = 0.11$, $A_{6,8} = 0.093$ (Fig. 3b). The mean value of the cells belonging to the cortico-hippocampal correlation is 0.70 whereas the mean value of the rest of the cells of **A** is -0.0091. This difference is highly significative (p=0.0004). This result confirms, in an unbiased way, that connectivity changes in the hippocampo-cortical correlation are a major consequence of scopolamine treatment and raise the possibility that they can serve as a relevant discriminatory factor for the reliable detection of scopolamine-induced pharmacological states (i.e. the ensemble of functional connectivity alterations) in a reduced number of experimental animals.

We then validated this model in evaluating the "scopolamine score" of the connectivity matrices before (baseline state) and after injection of scopolamine of a second cohort of mice, independent from the first one, that had followed the same pharmacological protocol. Remarkably, the SVM linear model was still able to reliably differentiate (p=0.0004) the two pharmacological states, yielding a score of -0.2 for the baseline matrices and 0.69 for the scopolamine matrices (Fig. 3c.d).

Next, in order to test the robustness of the classification performance, we used cross-validation with 100 iterations (Fig. 4). Notably, the mean SVM-coefficients matrix over those 100 iterations yielded again the highest values for the cells of the cortico-hippocampal correlation ($A_{2,7} = 0.079$, $A_{3,7} = 0.076$, $A_{4,7} = 0.079$, $A_{6,7} = 0.044$, $A_{2,8} = 0.080$, $A_{3,8} = 0.11$, $A_{6,8} = 0.093$). The excellent performance of the cross-validation test (AUC = 0.97 ± 0.03, Accuracy = 95% ± 4%, Sensitivity = 94% ± 8%, Specificity = 95% ± 7%) further validated the robustness of the SVM classification approach.

These results demonstrate the ability and robustness of the SVM regression model to automatically determine the pharmacological state of mice (i.e. baseline vs. scopolamine-treated), by using sparse training data.

3.3. Pharmacological validation for the automatic detection of scopolamine-induced connectivity changes

For the pharmacological validation of the score-based automatic detection method of scopolamine-induced connectivity changes, described above, we next investigated the dose-dependency of score values on six different awake mice cohorts injected at different scopolamine doses (see Methods.) We also evaluated the effects of post-scopolamine treatment with the the muscarinic acetylcholine receptor agonist milameline and the effects of a peripherically-restricted scopolamine derivative, methyl-scopolamine (Andrews et al., 1994). We used the regression model presented above to evaluate the pharmacological score for each group (Fig. 5.b).

As expected, the score of baseline time periods was low ($score_{baseline\_group\ 0} = -0.15$; $score_{baseline\_group\ 1} = -0.066$; $score_{baseline\_group\ 2} = -0.12$; $score_{baseline\_group\ 3} = -0.097$; $score_{baseline\_group\ 4} = -0.26$; $score_{baseline\_group\ 5} = -0.091$). No significant difference of the score was noticed after the injection of saline in group 0 ($score_{saline} = -0.17$), or after injection of scopolamine for group 1 ($score_{scop\ 0.1} = 0.35$) and group 2 ($score_{scop\ 0.2} = 0.13$) despite the increase of the scores for both of those two low-dose injected groups. Remarkably, from group 3 the scopolamine treated groups exhibit significantly higher scores: group 3 ($score_{scop\ 0.5} = 0.56$, significant increase compare to baseline: $p = 0.014$); group 4 ($score_{scop\ 3} = 0.61$, significant increase compare to baseline: $p = 0.003$). Nonetheless, these results indicate that the pharmacological score shows dose-dependent elevations, indicating pharmacological relevance. Importantly, changes in functional connectivity were not correlated with changes in global

cerebral blood flow (**Suppl. Fig.2**), as above. Furthermore, the score of group 5, treated by the peripherally restricted methyl-scopolamine was not significantly different from the score of baseline group, indicating that the scored brain connectivity changes require that scopolamine traverse the blood-brain barrier. Finally, treatment with the muscarinic acetylcholine receptor agonist milameline reverted the scopolamine-induced pharmacological score in each group near to baseline values: $score_{mila\_group\ 1} = 0.17$; $score_{mila\_group\ 2} = 0.23$; $score_{mila\_group\ 3} = 0.15$; $score_{mila\_group\ 4} = 0.19$; $score_{mila\_group\ 5} = 0.16$ further confirming pharmacological relevance. None of those scores is significantly different from their baseline reference.

Together, these results show that the functional connectivity data acquired with fUS imaging at a single coronal plane allows the establishment of a pharmacologically relevant score which is useful for efficient classification of treatment conditions, without any initial assumption, in a low number of animals.

4. Discussion

In this study we have first developed an experimental protocol for transcranial fUS imaging of functional connectivity in freely-moving awake-mice, which prevents confounding effects of anesthesia. Ultimately, this approach which uses a light ultrasonic probe, may be extended to functional imaging of brain activation and connectivity during behavioral essays.

Here we have used this setup for the imaging of functional connectivity changes induced by treatment with scopolamine, a muscarinic acetylcholine receptor antagonist and widely used reference drug for inducing cognitive deficits in healthy humans and animals (Klinkenberg and Blokland, 2010). We selected the functional connectivity time-domains where the ultrasonic cerebral signal resulting either from tissue signals or from blood flow signals can be discriminated. Qualitative evaluation indicated time-dependent changes of hippocampal and cortical connectivity following scopolamine application at the studied coronal slice. This was confirmed by unbiased selection of the most important connectivity changes by a machine-learning algorithm, which also provided a pharmacological score of scopolamine treatment after training in 5 experimental animals. Analysis of the connectivity matrices in an independent experimental cohort indicated that this "scopolamine score" is highly efficient for the classification of baseline vs. post-treatment brain states. Finally, pharmacological validation of the "scopolamine score" showed efficient measure of dose-dependent connectivity changes, followed by reversal of the score to baseline values by the muscarinic acetylcholine receptor agonist milameline, and the requirement for the penetration of scopolamine through the blood-brain barrier, as demonstrated by the lack of a significant score after administration of the peripherally-restricted methyl-scopolamine. Together, these results show that the functional connectivity data acquired with fUS imaging at a single coronal plane, non-invasively and in awake freely-moving mice without the bias of anesthesia, allows the establishment of a pharmacologically relevant score, which is useful for efficient classification of treatment conditions, without any initial assumption, in a low number of animals.

While we have previously demonstrated that fUS imaging is able measure the functional connectivity in anesthetized rats (Osmanski et al., 2014), subsequent experiments indicated that in mice the already significantly weaker functional connectivity is highly sensitive to standard anesthesia protocols (Ferrier et al., 2020), possibly explaining the relative paucity of functional connectivity studies in this major pre-clinical animal model. Our results indicate that fUS imaging in awake mice is able to reliably detect both functional connectivity at the resting-state, such as the characteristic bi-lateral connectivity patterns in the hippocampus and in the cortex in baseline acquisitions (Chuang and Nasrallah, 2017), and the pharmacologically-induced changes of these patterns.

Our results indicate that scopolamine-treatment leads to enhanced functional connectivity between the hippocampus and cortical regions, as indicated first qualitatively both by seed-based and ROI-based connectivity analysis and confirmed by the SVM linear model. According to (Mash and Potter, 1986) and (Schwab et al., 1992), M1 receptors are highly expressed in the isocortex and hippocampus while having a low expression level in the thalamus. Although scopolamine and milameline are not considered to be specific of any muscarinic receptor subtypes (Falsafi et al., 2012), our results seem to indicate a correlation between M1 receptors distribution and change in functional connectivity. This enhanced connectivity was visible after 10 minutes of subcutaneous scopolamine injection, was dose-dependent, could be rescued to baseline values by the muscarinic acetylcholine receptor agonist milameline, and was absent after treatment with the peripherally restricted scopolamine analogue, methyl-scopolamine. Contrary to previous studies (Méndez-López et al., 2011), we did not find significant thalamic changes in the left-right connectivity after scopolamine injections. This difference could be due to the small number of animals used for the present study or to the selected coronal plane.

Our results are in contradiction with the only study which investigated scopolamine-induced changes in rodent brain functional connectivity, by using BOLD-based fMRI (Shah et al., 2015). In this study a general decrease of functional connectivity was reported following scopolamine treatment. While both fMRI and fUS detect functional connectivity through the neurovascular coupling, important experimental differences may underlie these contradictory findings. First, while BOLD fMRI measures hemoglobin oxygenation as an indirect measure of blood flow changes, fUS directly measures cerebral blood volume with higher spatio-temporal resolution, leading to higher sensitivity (Boido et al., 2019), as discussed previously (Osmanski et al., 2014). Second, *Shah et al* used anaesthesia, which was shown to affect negatively functional connectivity strength (Chuang and Nasrallah, 2017). Combined, these differences may lead to a critical loss of detection sensitivity in the mouse brain, which, as compared to the larger rat brain, presents a challenge for fMRI imaging. A recent authoritative review (Chuang and Nasrallah, 2017) proposed that in order to be able to compare physiological condition and data quality across laboratories, the consistency in detecting the stereotypical connectivity patterns, such as the bi-lateral connectivity in the cortex or in the hippocampus, should be assessed similarly to the approach used in human studies to evaluate denoising methods for rsfMRI (Pruim et al., 2015). Notably, Shah et al. do not report stereotypical bi-lateral connectivity patterns, confirming the possibility of insufficient sensitivity. In contrast, fUS-based connectivity detection in awake mice consistently detects bi-lateral connectivity in the cortex or in the hippocampus as shown by Tiran et al. (Chuang and Nasrallah, 2017; Mechling et al., 2014; Osmanski et al., 2014) and in the present study (Fig. 2 and **Supplementary Fig.3**), similarly to recent high-sensitivity fMRI studies (Chuang and Nasrallah, 2017; Mechling et al., 2014).

What is the functional relevance of our results? In corresponding human cortical regions, early reports using positron emission tomography (PET) indicated hyperactivation following scopolamine injection, as indicated by elevated glucose consumption, a result that the authors considered as unexpected (Blin et al., 1995; Molchan et al., 1994). Concerning changes in connectivity, whereas topological similarity between human and mouse connectivity networks does not necessary imply functional similarity, it is notable that while human fMRI analysis of scopolamine-induced changes in functional connectivity in cortical regions also shows a general tendency for higher connectivity, with marked decrease in a subset of regions (Chhatwal et al., 2019), in the hippocampus scopolamine significantly enhanced cortico-hippocampal low-frequency coherence, similar to our results (Wink et al., 2006). In addition to fMRI-based approaches, human electroencephalography (EGG) studies have also reported scopolamine-induced increases in the power of low-frequency (delta and theta) activity, while alpha and beta-frequency activity were reduced (Alvarez-Jimenez et al., 2016; Ebert et al., 1998; Kikuchi et al., 1999; Liem-Moolenaar et al., 2011;

Sannita et al., 1987). Notably, low-frequency delta and theta EEG activity was found to correlate well with the resting-state functional MRI signal (Marawar et al., 2017), further suggesting pathophysiological relevance for our results, which show scopolamine-induced increase in cortico-hippocampal functional connectivity patterns. Notably, DFA (Detrended Fluctuation Analysis) of EEG signals in humans has also shown increased long-range correlations, in all frequency bands, after scopolamine injection (Simpraga et al., 2017). Such similarity in functional dysconnectivity in response to pharmacological manipulations indicate important translational potential, enabling the use of animal models as highly efficient tools to empirically test hypotheses on connectome involvement in brain dysfunction (Mp and O, 2019). Importantly, the scopolamine score could be reverted to normal values by milameline, providing a pharmacological rescue of a pathological index. In this context, the scopolamine score validated in our study may be used as a sensitive biomarker to detect dose-dependent effects of scopolamine on the brain, indicating important potential both for experimental pharmacology and drug development.

If this study proves the relevancy of functional ultrasound for pharmacological studies, we acknowledge that the limitation of the imaging modality in two dimensions can be bottleneck for the investigation of brain mechanisms without *a priori* information on the studied pathways. We recently introduced a proof-of-concept of 3D fUS neuroimaging in the rodent brain based on a 1024 channels research scanner and a matrix array probe (Rabut et al., 2019). Unfortunately, as of today, this method comes with a significant computational cost and typically yield reduced sensitivity or framerate compared to 2D fUS. However, we believe that the development of always more performant processor units will soon enable highly sensitive 3D fUS imaging to monitor brain mechanisms in the three dimensions. The advent of 3D fUS opens the possibility to record neurovascular dynamics of complete brain region volumes.

5. Conclusion

In conclusion, our study introduces fUS imaging, coupled to machine-learning based classification, as a highly sensitive and robust tool to detect pharmacologically-induced changes in brain connectivity patterns, without anesthesia bias. Potentially confounding vascular effects are controlled by real-time built-in monitoring of global brain perfusion. The pharmacological relevance of the pharmaco-fUS score is shown by its dose-dependency and sensitivity to antagonist pharmacological action. Our proof-of-concept demonstration of rescuing a pathological connectivity pattern by a pharmacological agent opens the way of using pharmaco-fUS as a physiologically relevant and clinically translatable read-out, both for basic neuroscience and for drug discovery.

Declaration of Competing Interest

T.D., M.T. and Z.L are co-founders and shareholders of Iconeus company commercializing ultrasound neuroimaging scanners.

CRediT authorship contribution statement

Claire Rabut: Data curation, Software, Methodology, Writing - original draft, Writing - review & editing. **Jérémy Ferrier:** Data curation, Writing - review & editing, Methodology. **Adrien Bertolo:** Software, Writing - review & editing. **Bruno Osmanski:** Software, Writing - review & editing. **Xavier Mousset:** Data curation, Software, Writing - review & editing. **Sophie Pezet:** Data curation, Methodology, Software, Writing - review & editing. **Thomas Deffieux:** Methodology, Software, Writing - review & editing. **Zsolt Lenkei:** Supervision, Conceptualization, Methodology, Writing - review & editing. **Mickaël Tanter:** Supervision, Conceptualization, Methodology, Writing - review & editing.

Acknowledgments

The research leading to these results has received funding from the European Research Council under the European Union's Seventh Framework Programme (FP7/2007-2013)/ERC Grand Agreement No. 339244-FUSIMAGINE, the LABEX WIFI (Laboratory of Excellence within the French Program 'Investments for the Future') under reference ANR-10-IDEX-0001-02 PSL, the National Agency for Research under the program 'future investments' with the reference ANR-10-EQPX-15 and the European program ANR-15-HBPR-0004-02 FUSIMICE of the Human Brain Project.

Supplementary materials

Supplementary material associated with this article can be found, in the online version, at doi:10.1016/j.neuroimage.2020.117231.

References

Alvarez-Jimenez, R., Groeneveld, G.J., Gerven, J.M.A.van, Goulooze, S.C., Baakman, A.C., Hay, J.L., Stevens, J., 2016. Model-based exposure-response analysis to quantify age related differences in the response to scopolamine in healthy subjects. Br. J. Clin. Pharmacol. 82, 1011–1021. https://doi.org/10.1111/bcp.13031.

Andrews, J.S., Jansen, J.H.M., Linders, S., Princen, A., 1994. Effects of disrupting the cholinergic system on short-term spatial memory in rats. Psychopharmacology (Berl.) 115, 485–494. https://doi.org/10.1007/BF02245572.

Blin, J., Chase, T.N., Piercey, M.F., 1995. Do the effects of muscarinic receptor blockade on brain glucose consumption mimic the cortical and subcortical metabolic pattern of Alzheimer's disease in normal volunteers ? In: Comar, D. (Ed.) PET for Drug Development and Evaluation, Developments in Nuclear Medicine. Springer, Netherlands, Dordrecht, pp. 123–132.

Boido, D., Rungta, R.L., Osmanski, B.-F., Roche, M., Tsurugizawa, T., Bihan, D.L., Ciobanu, L., Charpak, S., 2019. Mesoscopic and microscopic imaging of sensory responses in the same animal. Nat. Commun. 10, 1–13. https://doi.org/10.1038/s41467-019-09082-4.

Carmichael, O., Schwarz, A.J., Chatham, C.H., Scott, D., Turner, J.A., Upadhyay, J., Coimbra, A., Goodman, J.A., Baumgartner, R., English, B.A., Apolzan, J.W., Shankapal, P., Hawkins, K.R., 2018. The role of fMRI in drug development. Drug Discov. Today 23, 333–348. https://doi.org/10.1016/j.drudis.2017.11.012.

Cherry, S.R., 2001. Fundamentals of positron emission tomography and applications in preclinical drug development. J. Clin. Pharmacol. 41, 482–491. https://doi.org/10.1177/00912700122010357.

Chhatwal, J.P., Schultz, A.P., Hedden, T., Boot, B.P., Wigman, S., Rentz, D., Johnson, K.A., Sperling, R.A., 2019. Anticholinergic amnesia is mediated by alterations in human network connectivity architecture. Cereb. Cortex 29, 3445–3456. https://doi.org/10.1093/cercor/bhy214.

Chuang, K.-H., Nasrallah, F.A., 2017. Functional networks and network perturbations in rodents. NeuroImage 163, 419–436. https://doi.org/10.1016/j.neuroimage.2017.09.038.

Demené, C., Deffieux, T., Pernot, M., Osmanski, B.-F., Biran, V., Gennisson, J.-L., Sieu, L.-A., Bergel, A., Franqui, S., Correas, J.-M., Cohen, I., Baud, O., Tanter, M., 2015. Spatiotemporal clutter filtering of ultrafast ultrasound data highly increases doppler and fultrasound sensitivity. IEEE Trans. Med. Imaging 34, 2271–2285. https://doi.org/10.1109/TMI.2015.2428634.

Deng, G., Wu, C., Rong, X., Li, S., Ju, Z., Wang, Y., Ma, C., Ding, W., Guan, H., Cheng, X., Liu, W., Wang, C., 2019. Ameliorative effect of deoxyvasicine on scopolamine-induced cognitive dysfunction by restoration of cholinergic function in mice. Phytomedicine 63, 153007. https://doi.org/10.1016/j.phymed.2019.153007.

Deutsch, J.A., 1971. The cholinergic synapse and the site of memory. Science 174, 788–794. https://doi.org/10.1126/science.174.4011.788.

Dizeux, A., Gesnik, M., Ahnine, H., Blaize, K., Arcizet, F., Picaud, S., Sahel, J.-A., Deffieux, T., Pouget, P., Tanter, M., 2019. Functional ultrasound imaging of the brain reveals propagation of task-related brain activity in behaving primates. Nat. Commun. 10, 1–9. https://doi.org/10.1038/s41467-019-09349-w.

Ebert, U., Siepmann, M., Oertel, R., Wesnes, K.A., Kirch, W., 1998. Pharmacokinetics and pharmacodynamics of scopolamine after subcutaneous administration. J. Clin. Pharmacol. 38, 720–726. https://doi.org/10.1002/j.1552-4604.1998.tb04812.x.

Falsafi, S.K., Deli, A., Höger, H., Pollak, A., Lubec, G., 2012. Scopolamine administration modulates muscarinic, nicotinic and nmda receptor systems. PLoS ONE 7. https://doi.org/10.1371/journal.pone.0032082.

Ferrier, J., Tiran, E., Deffieux, T., Tanter, M., Lenkei, Z., 2020. Functional imaging evidence for task-induced deactivation and disconnection of a major default mode network hub in the mouse brain. Proc. Natl. Acad. Sci.. 201920475 https://doi.org/10.1073/pnas.1920475117 .

Guo, C., Shen, J., Meng, Z., Yang, X., Li, F., 2016. Neuroprotective effects of polygalacic acid on scopolamine-induced memory deficits in mice. Phytomedicine 23, 149–155. https://doi.org/10.1016/j.phymed.2015.12.009.

Haider, S., Tabassum, S., Perveen, T., 2016. Scopolamine-induced greater alterations in neurochemical profile and increased oxidative stress demonstrated a better model of dementia: a comparative study. Brain Res. Bull. 127, 234–247. https://doi.org/10.1016/j.brainresbull.2016.10.002.

Halldin, C., Gulyas, B., Farde, L., 2001. PET studies with carbon-11 radioligands in neuropsychopharmacological drug development. Curr. Pharm. Des. 7, 1907–1929. https://doi.org/10.2174/1381612013396871.

Ketih Franlkin, G.P., 2011. Paxinos and Franklin's the Mouse Brain in Stereotaxic Coordinates. Academic Press.

Kikuchi, M., Wada, Y., Nanbu, Y., Nakajima, A., Tachibana, H., Takeda, T., Hashimoto, T., 1999. EEG changes following scopolamine administration in healthy subjects. Neuropsychobiology 39, 219–226. https://doi.org/10.1159/000026588.

Klinkenberg, I., Blokland, A., 2010. The validity of scopolamine as a pharmacological model for cognitive impairment: A review of animal behavioral studies. Neurosci. Biobehav. Rev. 34, 1307–1350. https://doi.org/10.1016/j.neubiorev.2010.04.001.

Lee, J.-C., Park, J.H., Ahn, J.H., Park, J., Kim, I.H., Cho, J.H., Shin, B.N., Lee, T.-K., Kim, H., Song, M., Cho, G.-S., Kim, D.W., Kang, I.J., Kim, Y.-M., Won, M.-H., Choi, S.Y., 2018. Effects of chronic scopolamine treatment on cognitive impairment and neurofilament expression in the mouse hippocampus. Mol. Med. Rep. 17, 1625–1632. https://doi.org/10.3892/mmr.2017.8082.

Lee, J.-S., Hong, S.-S., Kim, H.-G., Lee, H.-W., Kim, W.-Y., Lee, S.-K., Son, C.-G., 2016. Gongjin-Dan enhances hippocampal memory in a mouse model of scopolamine-induced amnesia. PLoS ONE 11. https://doi.org/10.1371/journal.pone.0159823.

Liem-Moolenaar, M., Boer, P.de, Timmers, M., Schoemaker, R.C., Hasselt, J.G.C.van, Schmidt, S., Gerven, J.M.A.van, 2011. Pharmacokinetic–pharmacodynamic relationships of central nervous system effects of scopolamine in healthy subjects. Br. J. Clin. Pharmacol. 71, 886–898. https://doi.org/10.1111/j.1365-2125.2011.03936.x.

Lin, J., Huang, L., Yu, J., Xiang, S., Wang, J., Zhang, J., Yan, X., Cui, W., He, S., Wang, Q., 2016. Fucoxanthin, a marine carotenoid, reverses scopolamine-induced cognitive impairments in mice and inhibits acetylcholinesterase in vitro. Mar. Drugs 14, 67. https://doi.org/10.3390/md14040067.

Macé, E., Montaldo, G., Cohen, I., Baulac, M., Fink, M., Tanter, M., 2011. Functional ultrasound imaging of the brain. Nat. Methods 8, 662–664. https://doi.org/10.1038/nmeth.1641.

Mace, E., Montaldo, G., Osmanski, B.-F., Cohen, I., Fink, M., Tanter, M., 2013. Functional ultrasound imaging of the brain: theory and basic principles. IEEE Trans. Ultrason. Ferroelectr. Freq. Control 60, 492–506. https://doi.org/10.1109/TUFFC.2013.2592.

Marawar, R.A., Yeh, H.J., Carnabatu, C.J., Stern, J.M., 2017. Functional MRI correlates of resting-state temporal theta and delta eeg rhythms. J. Clin. Neurophysiol. 34, 69–76. https://doi.org/10.1097/WNP.0000000000000309.

Mash, D.C., Potter, L.T., 1986. Autoradiographic localization of M1 and M2 muscarine receptors in the rat brain. Neuroscience 19, 551–564. https://doi.org/10.1016/0306-4522(86)90280-0.

Mechling, A.E., Hübner, N.S., Lee, H.-L., Hennig, J., von Elverfeldt, D., Harsan, L.-A., 2014. Fine-grained mapping of mouse brain functional connectivity with resting-state fMRI. NeuroImage 96, 203–215. https://doi.org/10.1016/j.neuroimage.2014.03.078.

Méndez-López, M., Méndez, M., López, L., Arias, J.L., 2011. Memory performance and scopolamine: hypoactivity of the thalamus revealed by cytochrome oxidase histochemistry. Acta Histochem 113, 465–471. https://doi.org/10.1016/j.acthis.2010.04.004.

Molchan, S.E., Matochik, J.A., Zametkin, A.J., Szymanski, H.V., Cantillon, M., Cohen, R.M., Sunderland, T., 1994. A double FDG/PET study of the effects of scopolamine in older adults. Neuropsychopharmacology 10, 191–198. https://doi.org/10.1038/npp.1994.21.

Mp, van den, H., O, S., 2019. A cross-disorder connectome landscape of brain dysconnectivity. Nat. Rev. Neurosci. 20, 435–446. https://doi.org/10.1038/s41583-019-0177-6.

Muhammad, T., Ali, T., Ikram, M., Khan, A., Alam, S.I., Kim, M.O., 2019. Melatonin rescue oxidative stress-mediated neuroinflammation/ neurodegeneration and memory impairment in scopolamine-induced amnesia mice model. J. Neuroimmune Pharmacol. 14, 278–294. https://doi.org/10.1007/s11481-018-9824-3.

Nathan, P.J., Phan, K.L., Harmer, C.J., Mehta, M.A., Bullmore, E.T., 2014. Increasing pharmacological knowledge about human neurological and psychiatric disorders through functional neuroimaging and its application in drug discovery. Curr. Opin. Pharmacol., Neurosciences 14, 54–61. https://doi.org/10.1016/j.coph.2013.11.009.

Osmanski, B.-F., Pezet, S., Ricobaraza, A., Lenkei, Z., Tanter, M., 2014. Functional ultrasound imaging of intrinsic connectivity in the living rat brain with high spatiotemporal resolution. Nat. Commun. 5, 1–14. https://doi.org/10.1038/ncomms6023.

Park, H.R., Lee, H., Park, H., Cho, W.-K., Ma, J.Y., 2016. Fermented sipjeondaebo-tang alleviates memory deficits and loss of hippocampal neurogenesis in scopolamine-induced amnesia in mice. Sci. Rep. 6, 22405. https://doi.org/10.1038/srep22405.

Piel, M., Vernaleken, I., Rösch, F., 2014. Positron emission tomography in CNS drug discovery and drug monitoring. J. Med. Chem. 57, 9232–9258. https://doi.org/10.1021/jm5001858.

Pruim, R.H.R., Mennes, M., Buitelaar, J.K., Beckmann, C.F., 2015. Evaluation of ICA-AROMA and alternative strategies for motion artifact removal in resting state fMRI. NeuroImage 112, 278–287. https://doi.org/10.1016/j.neuroimage.2015.02.063.

Rabut, C., Correia, M., Finel, V., Pezet, S., Pernot, M., Deffieux, T., Tanter, M., 2019. 4D functional ultrasound imaging of whole-brain activity in rodents. Nat. Methods 16, 994–997. https://doi.org/10.1038/s41592-019-0572-y.

Sannita, W.G., Maggi, L., Rosadini, G., 1987. Effects of scopolamine (0.25–0.75 mg i.m.) on the quantitative EEG and the neuropsychological status of healthy volunteers. Neuropsychobiology 17, 199–205. https://doi.org/10.1159/000118365.

Schwab, C., Brückner, G., Rothe, T., Castellano, C., Oliverio, A., 1992. Autoradiography of muscarinic cholinergic receptors in cortical and subcortical brain regions of C57BL/6 and DBA/2 mice. Neurochem. Res. 17, 1057–1062. https://doi.org/10.1007/BF00967281.

Shah, D., Blockx, I., Guns, P.-J., De Deyn, P.P., Van Dam, D., Jonckers, E., Delgado y Palacios, R., Verhoye, M., Van der Linden, A., 2015. Acute modulation of the cholinergic system in the mouse brain detected by pharmacological resting-state functional MRI. NeuroImage 109, 151–159. https://doi.org/10.1016/j.neuroimage.2015.01.009.

Sieu, L.-A., Bergel, A., Tiran, E., Deffieux, T., Pernot, M., Gennisson, J.-L., Tanter, M., Cohen, I., 2015. EEG and functional ultrasound imaging in mobile rats. Nat. Methods 12, 831–834. https://doi.org/10.1038/nmeth.3506.

Simpraga, S., Alvarez-Jimenez, R., Mansvelder, H.D., Gerven, J.M.A.van, Groeneveld, G.J., Poil, S.-S., Linkenkaer-Hansen, K., 2017. EEG machine learning for accurate detection of cholinergic intervention and Alzheimer's disease. Sci. Rep. 7, 1–11. https://doi.org/10.1038/s41598-017-06165-4.

Sperling, R., Greve, D., Dale, A., Killiany, R., Holmes, J., Rosas, H.D., Cocchiarella, A., Firth, P., Rosen, B., Lake, S., Lange, N., Routledge, C., Albert, M., 2002. Functional MRI detection of pharmacologically induced memory impairment. Proc. Natl. Acad. Sci. 99, 455–460. https://doi.org/10.1073/pnas.012467899.

Tiran, E., Ferrier, J., Deffieux, T., Gennisson, J.-L., Pezet, S., Lenkei, Z., Tanter, M., 2017. Transcranial functional ultrasound imaging in freely moving awake mice and anesthetized young rats without contrast agent. Ultrasound Med. Biol. 43, 1679–1689. https://doi.org/10.1016/j.ultrasmedbio.2017.03.011.

Wandschneider, B., Koepp, M.J., 2016. Pharmaco fMRI: Determining the functional anatomy of the effects of medication. NeuroImage Clin 12, 691–697. https://doi.org/10.1016/j.nicl.2016.10.002.

Wink, A.M., Bernard, F., Salvador, R., Bullmore, E., Suckling, J., 2006. Age and cholinergic effects on hemodynamics and functional coherence of human hippocampus. Neurobiol. Aging 27, 1395–1404. https://doi.org/10.1016/j.neurobiolaging.2005.08.011.

Xu, H., You, Z., Wu, Z., Zhou, L., Shen, J., Gu, Z., 2016. WY14643 Attenuates the Scopolamine-Induced Memory Impairments in Mice. Neurochem. Res. 41, 2868–2879. https://doi.org/10.1007/s11064-016-2002-1.